Water Adsorption on the β-Dicalcium Silicate Surface from DFT Simulations: a Dual Nucleophilic-Electrophilic Interaction

Qianqian Wang,[1] **Hegoi Manzano,**[2]* **Iñigo López-Arbeloa,**[3] **and Xiaodong Shen**[1]*

[1] State Key Laboratory of Materials-Oriented Chemical Engineering, College of Materials Science and Engineering, Nanjing Tech University, Nanjing 210009, China.
[2] Condensed Matter Physics Department, University of the Basque Country, UPV/EHU, 48080, Bilbao, Spain
[3] Molecular Spectroscopy Laboratory, Department of Physical Chemistry, University of the Basque Country, UPV/EHU, 48080, Bilbao, Spain

* Correspondence: hegoi.manzano@ehu.eus, xdshen@njtech.edu.cn

Abstract: β-dicalcium silicate (β-Ca$_2$SiO$_4$, or β-C$_2$S in cement chemistry notation) is one of the most important minerals in cement. An improvement of its hydration speed would be the key point for developing environmentally friendly cements with lower energy consumption and CO$_2$ emissions. However, there is a lack of fundamental understanding on the water/β-C$_2$S surface interactions. Therefore, in this work we aim to understand the water adsorption and dissociation mechanism on the β-C$_2$S (100) surface using density functional theory (DFT) calculations. Our results indicate that thermodynamically favorable water adsorption process takes place in several surface sites, with a broad range of adsorption energies (-0.78 to -1.24 eV), depending on the particular water conformation and surface site. To clarify the key factor governing the adsorption, the electronic properties of water at the surface sites were analyzed. The partial density of states (DOS), charge analysis, and electron density difference analyses suggest a dual interaction of water with β-C$_2$S (100) surface: a nucleophilic interaction of the water oxygen lone pair with surface calcium atoms, and an electrophilic interaction (hydrogen bond) of one water hydrogen with surface oxygen atoms, being the first one the stronger interaction. Hence, we suggest that β-C$_2$S hydration could be enhanced by introducing chemical or structural changes that increase both the electronegative/positive character of the surface.

Keywords: Belite, Hydration, Density Functional Theory, Water Adsorption, Calcium Silicate

1. Introduction

Hydration and dissolution of crystals have a profound impact on a broad range of scientific and technological processes such as thermochemical energy storage [1,2], geochemical phenomena at the mineral/water interfaces [3,4], and durability of glasses and biomaterials [5,6]. A prominent technological application of crystal dissolution is the production of cement and concrete. Cement, as the "adhesive" in concrete, is used worldwide social infrastructures, military and civil buildings, being the most consumed manufactured material. The clinker hydration is the crucial step which controls the final properties of cement materials, and yet, the hydration process of cement minerals are still arguably despite the long lasting research [7]. Due to the large amount of CO$_2$ emissions and energy consumption in cement industry and the increasing demand, understanding cement

hydration mechanisms is urgently needed to supply an academic basis for the design of new environmentally friendly cements.

Belite (β-dicalcium silicate, β-C$_2$S in cement chemistry notation) is an artificial orthosilicate that forms during the sintering of cement clinker, yet it has a natural counterpart called Larnite [8] that appears in natural environments. It is one of the most important minerals in cement industry, and has potential advantages for achieving the low carbon emission goal due to its lower sintering temperature and low calcium carbonate resource demanding compared to tricalcium silicate, the base component of traditional cements. However, the low hydration rate of belite restricts its engineering applications. Until now, the experimental endeavours conducted to improve its hydration [9–12] have had a very limited success.

In such scenario, atomistic simulations are a valuable tool as a complement to experiments in order to study the hydration mechanism of materials, as they have demonstrated for ionic solids [13], metallic oxides [14,15], minerals [16–18], or ceramics [19]. Regarding cement, atomistic simulations have been mainly used to investigate tricalcium silicate [20–26], the main component of cement, and much less attention has been paid to β-C$_2$S [27–29]. In this article we aim to investigate the interaction between β-C$_2$S surface and water molecules from a fundamental point of view, using Density Functional Theory (DFT) simulations. The obtained results will help us to understand the factors that govern β-C$_2$S/water interaction, and let us suggest routes to enhance its hydration kinetics.

2. Materials and Methods

2.1. Model Construction

The crystal structure of β-C$_2$S resolved by Mumme [30] was used as the starting point. Based on previous DFT studies [27,28], we decided to use the (100) surface to investigate the water dissociation process. Compare to other lower index cleavages, it has the second lowest cleavage energy, just 0.09 eV higher than the most stable cleavage (101), and 0.14 eV lower than the third most stable cleavage (010). Analyzing the crystal Wulff's crystal reconstruction, showed in the appendix A, we observed that the contribution of the (100) surface to the equilibrium shape's total surface area is 20%, just 2% and 1% smaller than the (101) and (010) surfaces respectively. We do not expect neither a radical different behavior of water adsorption on this surface nor in the crystal hydration due to their comparable properties. However, the (100) surface presents all the atom types with different equivalent positions defined by symmetry exposed to the vacuum, so it can be considered as a good representative cleavage. A slab with dimensions 13.5 Å x 18.6 Å in the periodic directions and 20 Å thick was constructed, with a vacuum layer set to be 16 Å, as shown in Fig.1 (a).

2.2. Computational details

The DMol3 density functional theory (DFT) package [31] was employed to study the interaction between the slab model and water. The exchange-correlation is treated in the generalized gradient approximation (GGA) with the Perdew-Burke-Ernzerhof (PBE) functional [32]. The treatment for the core electrons is all electrons method. A double ζ plus polarization (DZP) basis set is used, with a global orbital cut-off radius of 5.5 Å. The orbital smearing parameter is set to 0.01 eV to balance precision and computing performance. The k-point grid in the first Brillouin zone is constructed using the Monkhorst-Pack method [33], with a 2×2×1 k-points grid. Self-consistent iteration convergence precision is set to 2.5×10^{-5} eV, the energy convergence tolerance to 2.5×10^{-4} eV, and the maximum stress is set to be lower than 0.05 eV/Å. During surface relaxation process a maximum displacement of atoms of 0.005 Å at each step was allowed, and the middle of slab (6.5 Å from each surface) atoms were fixed. Furthermore, an external additional potential was applied to correct macroscopic dipole formation [34].

89   Fig. 1(a) depicts the relaxed β-C2S (100) surface model described in Section 2.1, together with (b)
90   the projection of the electrostatic potential along the perpendicular direction to the surface. The
91   electrostatic potentials of the upper and bottom surfaces are symmetrical, with a considerable change
92   at the interface where it becomes wider as it extends to the vacuum region. In the middle of vacuum
93   layer, the electrostatic potential matches the vacuum level energy, which indicates that there is no
94   interaction between the upper and lower surfaces. Therefore, the vacuum layer thickness choice is
95   enough to avoid self-interactions.
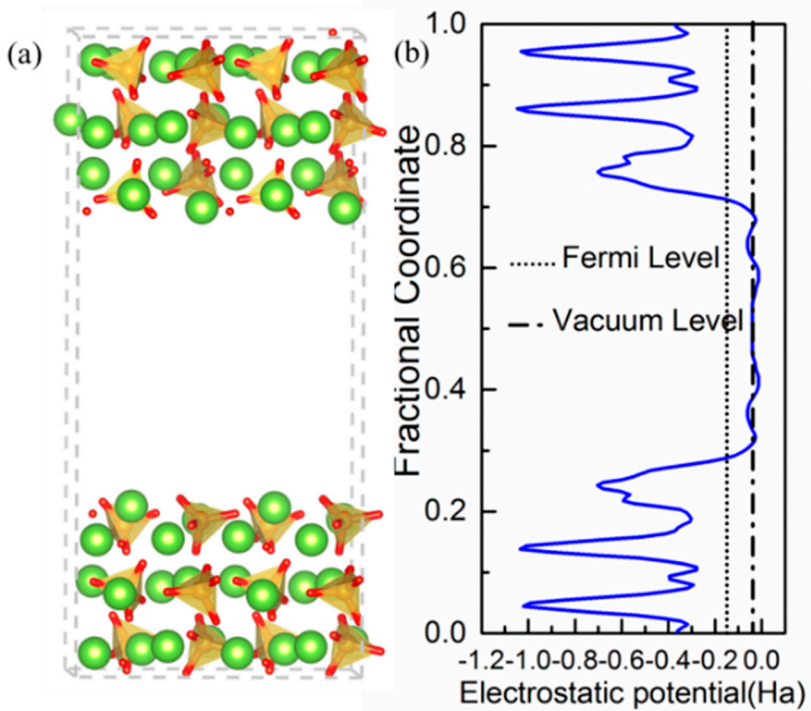
96
97   **Figure 1 (a)** Atomic representation of the β-C2S (100) surface model visualized with VESTA[35]. Red, green and
98   orange spheres represent oxygen, calcium and silicate atoms, respectively. The SiO_4^{-4} groups are further
99   represented as orange tetrahedra. **(b)** Electrostatic potentials along with the vertical vectors of the slab. The solid
100   line represents the vacuum level.
101

102   **3. Results**

103   *3.1. Water adsorption conformation on β-C2S (100) surface and bonding scheme*

104   The surface structure of β-C2S is quite irregular, with Ca and O ions of different symmetry
105   present, silicate ions arranged with different orientations, and a considerable roughness. Therefore,
106   it is more difficult to define "a priori" the water adsorption points on the surface than for symmetrical
107   metal oxides, such as TiO_2, CaO , MgO [14,36,37], or two-dimensional materials, such as Ti2C [19]. In
108   a previous work [28], water adsorption sites were exhaustively searched using empirical force field
109   methods. Using that information, we have targeted the most favourable adsorption sites of water at
110   β-C2S, performing an energy minimization on the force field final configuration for each adsorption
111   configuration. It must be noted that the conformation at sites labelled as W2 and W4 were different
112   in the empirical simulation, yet after the present DFT energy minimization they became equivalent.

113   The investigated sites are shown in Fig. 2, and the corresponding adsorption energies in Table
114   1. In general, water is adsorbed in a configuration with the oxygen atom O(w) coordinated to surface
115   calcium atoms Ca, and one of its hydrogen atoms H(w) pointing towards the surface, forming a
116   hydrogen bond with oxygen atoms O(s) from the surface silicate groups. The adsorption energies
117   vary in a range from -0.78 to -1.24 eV, which indicates that the surface is considerably hydrophilic

118   and adsorption energetically favourable [38]. In all the reported adsorption sites the water molecule
119   stablishes a single hydrogen bond with O(s) atoms, with bond lengths smaller than 1.6 Å and H(w)-
120   O(w)-O(s) angles below 24º. In water, hydrogen bond distances and angles are typically larger, about
121   1.9 Å and less than 35º respectively [39,40]. Since the hydrogen bond length and strength are usually
122   correlated [39] this suggests a strong hydrogen bond between water and belite surface. Regarding
123   the Ca-O(w) distance, we found that the coordination distances of Ca-O(w) on the interface are bellow
124   2.65 Å which match with the Ca-O coordination distance on bulk β-C2S [30].

125   Based on the described conformations we can suggest a bonding scheme in which β-C2S suffers
126   simultaneously both nucleophilic and electrophilic attack from water [22,29]: the Ca is an electron
127   acceptor from the O(w) electron donor, and the O(s) is an electron donor (or proton acceptor) to the
128   H(w) electron acceptor, forming a hydrogen bond. However, it is quite complex to correlate the
129   magnitude of the adsorption energy as a function of the conformation adopted by water at the
130   surface. Hence, it is necessary to analysis the electronic properties of the adsorbate/substrate system
131   to understand the water adsorption mechanism on the surface.

132
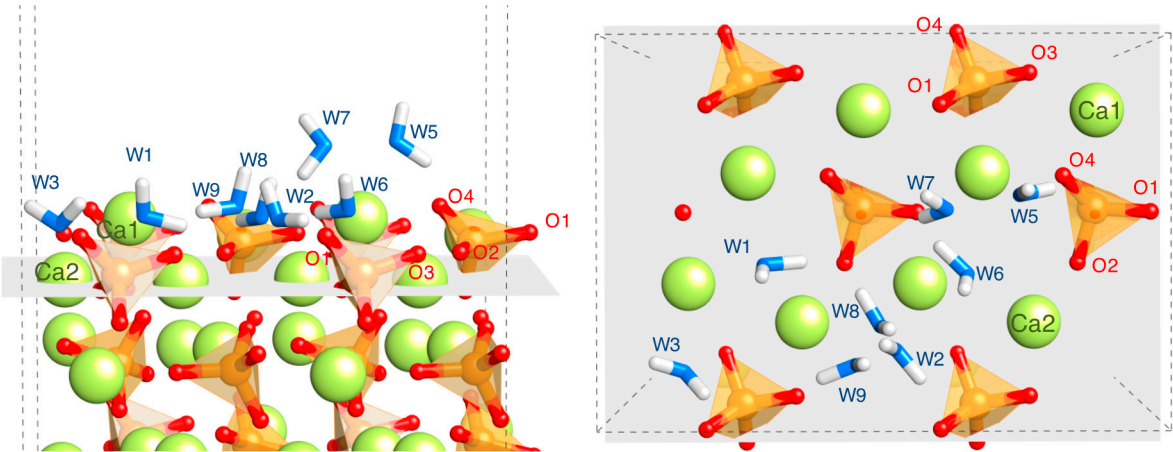
133   **Figure 2 .** Water adsorption configurations on the 9 adsorption sites of β-C2S (100) in side and top views. The
134   nomenclature of the Ca and O sites from dicalcium silicate follow that of the original paper describing the
135   crystalline structure [30]. The atoms representation is the same as in figure 1, including the water molecules with
136   the O atoms in blue and the H atoms in white.

137

138   **Table 1** Hirshfeld charge of water molecule atoms for various adsorption sites as well as the corresponding
139   adsorption energies. The adsorption sites are named from 1 to 9 in descending adsorption energy order, and the
140   surface Ca and oxygen numbers are thos in figure 2. The water molecule atoms are named with the w subscript.
141   The H_w taking part of the hydrogen bond (see text) is labeled as H_w (O)

No.	Adsorption Site	Adsorption Energy (eV)	Hirshfeld charge on water (e-)				Hirshfeld charge on surfaces (e-)		Bond distance Ca-Ow (Å)	Bond distance O-Hw (Å)
			O_w	$H_w(O)$	H_w	Total	Ca	O		
W1	Ca1 O4	-1.24	-0.198	0.099	0.180	0.081	0.612	-0.321	2.595	1.419
W2	Ca2 O3	-1.14	-0.195	0.108	0.181	0.094	0.477	-0.361	2.644	1.598
W3	Ca2 O3	-1.14	-0.196	0.107	0.179	0.09	0.475	-0.362	2.630	1.593
W4	Ca2 O3	-1.14	-0.198	0.106	0.179	0.087	0.476	-0.362	2.630	1.392
W5	Ca1 O2	-1.09	-0.269	0.101	0.169	0.001	0.649	-0.356	2.351	1.550
W6	Ca2 O1	-1.07	-0.218	0.095	0.176	0.053	0.446	-0.218	2.542	1.393
W7	Ca1 O1	-1.00	-0.258	0.108	0.174	0.024	0.649	-0.258	2.395	1.661
W8	Ca2 O4	-0.91	-0.203	0.103	0.177	0.077	0.462	-0.203	2.560	1.524
W9	Ca1 O1	-0.78	-0.207	0.122	0.182	0.097	0.498	-0.207	2.546	1.677

| H$_2$O | - | - | -0.302 | 0.151 | 0.151 | 0 | - | - | - | - |

142

3.2. Charge population analysis

A Hirshfield population analysis [41] was performed to investigate the atomic charge transfer between the water molecule and the surface. Table 1 gives the computed charges on the water molecule atoms for the adsorption sites as well as the charges on the surface atoms. Compared with the isolated water molecule, the absolute values of the Hirschfeld charges on the water oxygen atoms have decreased in all the adsorption configurations. It suggests electron transfer from O(w) to Ca(s) as we proposed before. Regarding the water hydrogen atoms, we can first observe an anisotropy in their charges, due to the formation of a single hydrogen bond between a water and surface oxygen atom. The H(w) involved in the hydrogen bond is an electron acceptor from the surface O(s), therefore decreasing its positive charge. The remaining hydrogen, pointing towards the vacuum, increases its charge, possible due to intramolecular electron withdraw from the O(w) which has donate electrons to the surface. The trend of the Hirshfeld population on the β-C$_2$S (100) surface atoms involved in the adsorption corroborate the changes described for the water molecules. There is a positive charge decrease on Ca(s) due to the electron transfer from O(w), and a negative charge decrease on the O(s) due to the electron transfer to the H(w).

The Hirshfeld population analysis interpretation matches with the proposed bonding scheme. Overall, there is a net positive charge on the adsorbed water molecule, which indicates that the electron depletion of the O(w) donnor is more important that the electron surfeit of the H(w). If we consider that the binding energy due to the hydrogen bond represents about 0.22 eV, similar to the one between water molecules [42,43], it is clear that most of the adsorption energy gain arises from the O(w)-Ca ionic interaction. Hence, the population analysis suggests that the main interaction in the water adsorption is the O(w)-Ca ionic interaction.

3.3. Partial Density of States

Hirshfeld population analysis reveals a net electron transfer from the water molecules to the surface. For further understanding of the process, the partial density of states (PDOS) of the Ca(s) and O(s) atoms involved in the highest adsorption energy site (W1) and the lowest adsorption energy site (W9) are investigated, before and after water adsorption. In both sites, the p-orbitals from surface O atoms are the most significant states contributing to the valence band maximum (VBM). This indicates that the under coordinated dangling oxygen atoms on the surface localize the electronic charge, being susceptible for suffering electrophilic attack from water and donate electrons. Regarding the conduction band minimum (CBM), there is a larger contribution of Ca1-s unoccupied states in the of W1 and W9 sites. Hence, the surface Ca atoms are prone of suffering nucleophilic attack and accept electrons. Therefore, the PDOS of the bare surface matches again with the suggested bonding scheme. Overall, the contribution of oxygen p-states to the VBM and the calcium s-states to the CBM is stronger in the W1 sites, which makes them more favorable both for electrophilic and nucleophilic attack, a perfect situation for the adsorption of water molecules, as can be seen from its corresponding adsorption energy.

After water chemisorption, the orbitals of the water molecule are hybridized with both O-p VBM and Ca-s CBM states of the surfaces as shown in fig. 3(c) and (d), respectively. The effect of water is stronger in the CBM than in the VBM, which suggest the Ca-water interaction contributes to the adsorption stabilization more than the hydrogen bond. Furthermore, in the W1 site the CBM is distributed both in the Ca-s and H(w) unoccupied states, while in the W9 it is strongly localized in the water hydrogen atoms. This suggests that the H(w) in the W9 has not established a strong hydrogen bond with the O(s), and therefore still has the capacity to accept electrons. In fact, the

187 Hirsfeld charge on the H(w) at the W9 site has suffer the lower decrease with respect to the isolated
188 water, confirming this interpretation. Again, these findings agree with the bonding scheme proposed
189 from previous analysis, and give an explanation of the more favourable water adsotpion in   W1 than
190 W9 sites.

191
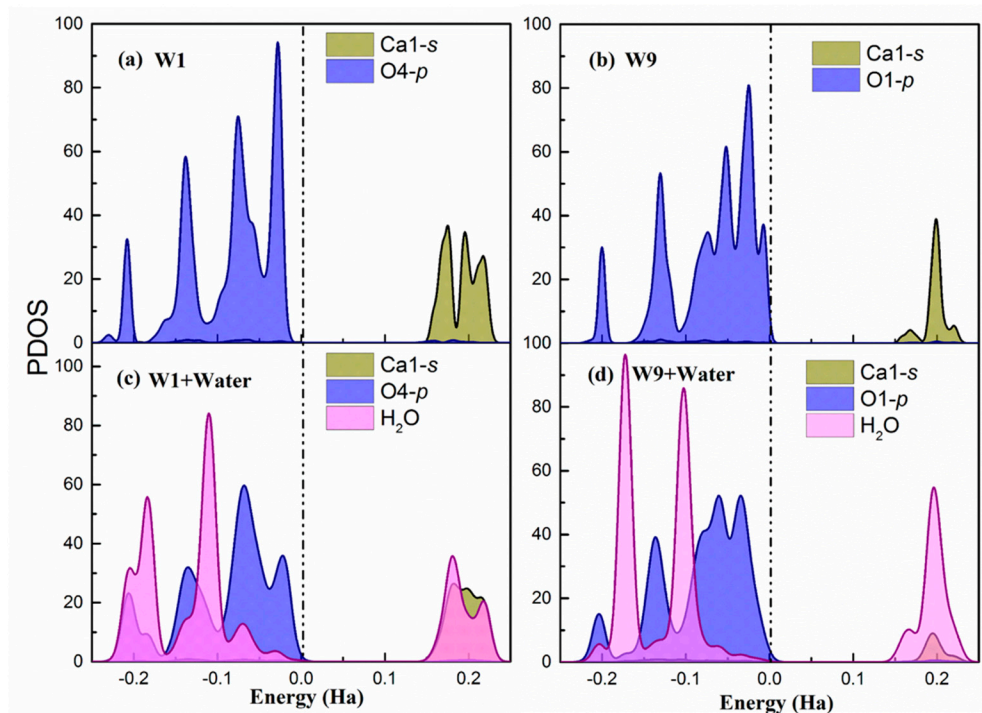
192 **Figure 3.** (a) and (b) The partial density of states of W1 and W9 adsorption sites on the relaxed surface; (c) and
193 (d) The partial density of states of W1 and W9 adsorption sites after water adsorbed on the surface. The dash
194 dot line indicates the Fermi level.

195 *3.4 Chemical bonding from charge density difference analysis*

196   To complete the characterization of chemical bonding and charge transfer, we move forward to
197 study the spatial electron density distribution before and after the water adsorption from electron
198 density difference, $\Delta\rho$, calculated from the formula:

$$\Delta\rho = (\rho_{H_2O} + \rho_{surf}) - \rho_{H_2O+surf} \tag{1}$$

199 where $\rho_{H2O+surf}$ represents the electron density distribution of the water adsorbed on the surface; ρ_{H2O}
200 and ρ_{surf} are the electron densities of individual water molecules and pure surface respectively.
201 Accordingly, a positive $\Delta\rho$ value in a point indicate a lower electronic density after water adsorption
202 due to electron density depletion, and negative values a higher electronic density due to electron
203 density surfeit. The electron density difference was plotted in Fig. 4, where light and dark blue
204 isosurfaces represent the $\Delta\rho < 0$ and > 0 respectively.

205   It can be observed that the electron density around the adsorption points of the surface is
206 significantly polarized after the water adsorption, yet the effect is local and only the atoms involved
207 in the adsorption site are affected. In both cases the situation is similar: there is a localized electronic
208 density depletion in the O(s) atoms that forms the hydrogen bond, as well as a more delocalized
209 depletion in the area of the water oxygen lone pair. On the other hand, the electronic density
210 increment on the H(w) atoms, and the Ca(s) atoms shown in Fig. 4(c) and 4(d). It must be noted that
211 the electron density surfeit takes place in more than one Ca atoms from the surface, so the adsorption
212 site involves an ionic interaction with more than one Ca atom from the surface. From the charge
213 density isosurfaces, it is apparent that the charge transfer is more pronounced on the W1 sites in

214　comparison with the W9 sites, which is in agreement with the Hirshfeld populations, the PDOS
215　analysis, and the computed adsorption energies.

216　　Once more, the findings are consistent with the suggested electrophilic-nucleophilic dual
217　adsorption scheme, i.e., the H(w) being an electron acceptor from the surface O and the O(w) being
218　an electron donor to surface Ca atoms.

219
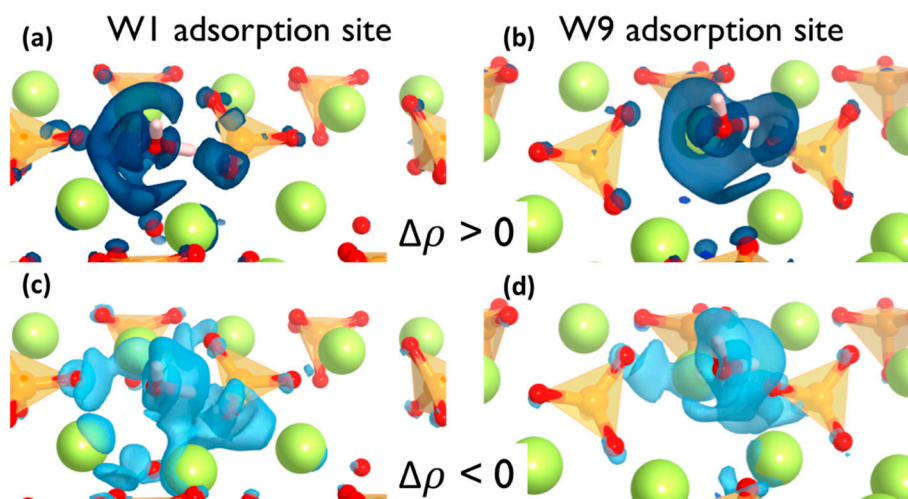
220　**Figure 4.** Isosurface plots of the electron density difference for W1 (a,c) and W9 (b,d) adsorption sites. Dark and
221　light blue isosurfaces indicate the electron density depletion and surfeit, respectively.

4. Conclusions

223　　β-dicalcium silicate is a promising candidate to develop low-CO2 cements, yet its slow hydration
224　rate has limited its practical applications so far. In this work density functional theory simulations
225　have been employed with the aim of understanding the water adsorption mechanism on β-dicalcium
226　silicate (100) surface, and suggest possible routes to enhance its reactivity.

227　　Due to the structural complexity, there are multiple water adsorption sites with different
228　energies on β-C2S (100) surface. The most favourable adsorption sites are ascribed to the co-existence
229　of a dangling oxygen atom from the silicate group and surface calcium atoms. The structural and
230　electronic analyses point towards a double nucleophilic-electrophilic attack by water molecules to
231　the β-C2S (100) surface: On the one hand, there is electron transfer from the water molecule oxygen
232　atom to the surface Ca atoms. On the other hand, one of the water hydrogen atoms establishes a
233　hydrogen bond with the silicate oxygen atoms along with transferring positive charge onto the
234　silicate oxygen atoms. Among these two possibilities, the electronic structure analysis suggests that
235　the interaction between water and the β-C2S (100) adsorption sites is predominantly governed by the
236　Ca (surface)-O (water) ionic interaction, in which the surface calcium atoms acts as positive charge
237　donor (electron acceptor) with the interaction of the O(w) lone pair. In contrast, the hydrogen bond
238　interaction plays a less important role.

239　　These findings are the first step towards rational design high reactive belite crystals. Specifically,
240　we suggest that Frenkel or Schottky point defects could increase the donor and acceptor character of
241　the atoms close to the vacancy, enhancing the interaction with water. Similarly, isovalent chemical
242　substitutions of Ca or O by more electropositive and electronegative atoms, or aliovalent
243　substitutions, should create favourable points for water nucleophilic-electrophilic dual interaction. It
244　must be taken into account that the point defects will enhane local affinity for water, yet macroscopic
245　hydration should be also influenced by line, plane, and bulk defects [7,44].

Acknowledgments: The authors thank the supports of the Project Funded by the National Natural Science Foundation of China (No. 51602148), the Priority Academic Program Development of Jiangsu Higher Education Institutions (PAPD), the Program for Innovative Research Team in University of Ministry of Education of China (No.IRT_15R35), the financial support from the Departamento de Educación, Política Lingüística y Cultura del Gobierno Vasco (IT912-16) and the ELKARTEK project. The technical and human support provided by IZO-SGI SGIker of UPV/EHU and European funding (ERDF and ESF) is also acknowledged.

Author Contributions: "Q.W., H.M. and X.S. conceived and designed the simulations; Q.W. performed the simulations; Q.W. and H.M. analyzed the data; Q.W., H.M. and I.L.wrote the paper."

Appendix A
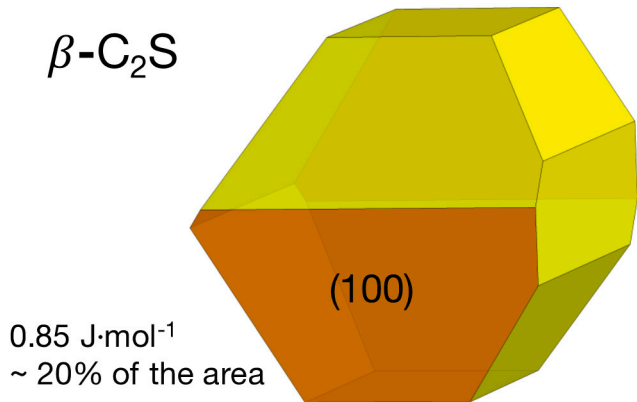
Figure S1. Wulff shape reconstruction of β-C$_2$S according to the surfaces energies computed in ref. [28]. The 3 labeled surfaces are the main surfaces in terms of contribution to the total area, and the label shows their cleavage, their contribution to the total surface, and their surface energies. The shape reconstruction and the contribution of each surface to the total area of the crystal has been obtained from the VESTA code [35].

Appendix B

Table B1. Hirshfeld atomic charges on the water and surface atoms for the studied adsorption configurations. The Hw taking part of the hydrogen bond is labeled as Hw (O)

No.	Adsorption Sites	Adsorption Energy (eV)	Hirshfeld charge on water				Hirshfeld charge on surfaces	
			Ow	Hw (O)	Hw	Total	Ca (e)	Os (e)
W1	Ca1 O4	-1.24	-0.198	0.099	0.180	0.081	0.612	-0.321
W2	Ca2 O3	-1.14	-0.195	0.108	0.181	0.094	0.477	-0.361
W3	Ca2 O3	-1.14	-0.196	0.107	0.179	0.09	0.475	-0.362
W4	Ca2 O3	-1.14	-0.198	0.106	0.179	0.087	0.476	-0.362
W5	Ca1 O2	-1.09	-0.269	0.101	0.169	0.001	0.649	-0.356
W6	Ca2 O1	-1.07	-0.218	0.095	0.176	0.053	0.446	-0.218
W7	Ca1 O1	-1.00	-0.258	0.108	0.174	0.024	0.649	-0.258
W8	Ca2 O4	-0.91	-0.203	0.103	0.177	0.077	0.462	-0.203
W9	Ca1 O1	-0.78	-0.207	0.122	0.182	0.097	0.498	-0.207
H2O	-	-	-0.302	0.151	0.151	0	-	-
C2S	Ca1						0.666	
C2S	Ca2						0.511	
C2S	O1							-0.398
C2S	O2							-0.411
C2S	O3							-0.412
C2S	O4							-0.380
Average charge variation			0.086	-0.046	0.026	0.067	-0.036	0.045

266   **Appendix C**

267
268   **Table C1.** Interatomic distances between water molecules and surface atoms and intramolecular bond distances
269   for the studied adsorption configurations. The H_w taking part of the hydrogen bond is labeled as H_w (O)
270

No.	Adsorption Sites	Adsorption Energy (eV)	Water-surface distances		Intramolecular distances	
			$Ca-O_wH_w$ (Å)	$O-H_w$ (Å)	$O_w-H_w(O)$ (Å)	O_w-H_w (Å)
W1	Ca1 O4	-1.24	2.595	1.419	0.99	0.85
W2	Ca2 O3	-1.14	2.644	1.598	1.08	0.84
W3	Ca2 O3	-1.14	2.630	1.593	1.07	0.88
W4	Ca2 O3	-1.14	2.630	1.392	1.06	0.83
W5	Ca1 O2	-1.09	2.351	1.550	1.01	0.76
W6	Ca2 O1	-1.07	2.542	1.393	0.95	0.81
W7	Ca1 O1	-1.00	2.395	1.661	1.08	0.81
W8	Ca2 O4	-0.91	2.560	1.524	1.03	0.81
W9	Ca1 O1	-0.78	2.546	1.677	1.22	0.84

271
272

273   **References**

274   1.   Cot-Gores, J.; Castell, A.; Cabeza, L. F. Thermochemical energy storage and conversion: A-state-of-the-art
275   review of the experimental research under practical conditions. *Renew. Sustain. Energy Rev.* **2012**, *16*, 5207–
276   5224, doi:10.1016/j.rser.2012.04.007.
277   2.   Sharma, A.; Tyagi, V. V; Chen, C. R.; Buddhi, D. Review on thermal energy storage with phase change
278   materials and applications. *Renew. Sustain. energy Rev.* **2009**, *13*, 318–345.
279   3.   Ohlin, C. A.; Villa, E. M.; Rustad, J. R.; Casey, W. H. Dissolution of insulating oxide materials at the
280   molecular scale. *Nat. Mater.* **2010**, *9*, 11–9, doi:10.1038/nmat2585.
281   4.   Brantley, S. L.; Kubicki, J. D.; White, A. F. *Kinetics of water-rock interaction*; Springer, 2008; Vol. 168;.
282   5.   Oelkers, E. H. General kinetic description of multioxide silicate mineral and glass dissolution. *Geochim.*
283   *Cosmochim. Acta* **2001**, *65*, 3703–3719, doi:10.1016/S0016-7037(01)00710-4.
284   6.   Porter, A. E.; Patel, N.; Skepper, J. N.; Best, S. M.; Bonfield, W. Comparison of in vivo dissolution processes
285   in hydroxyapatite and silicon-substituted hydroxyapatite bioceramics. *Biomaterials* **2003**, *24*, 4609–4620,
286   doi:10.1016/S0142-9612(03)00355-7.
287   7.   Bullard, J. W.; Jennings, H. M.; Livingston, R. A.; Nonat, A.; Scherer, G. W.; Schweitzer, J. S.; Scrivener, K.
288   L.; Thomas, J. J. Mechanisms of cement hydration. *Cem. Concr. Res.* **2011**, *41*, 1208–1223.
289   8.   Jost, K. H.; Ziemer, B.; Seydel, R.; H, K. Redetermination of structure of beta-dicalcium silicate. *Acta*
290   *Crystallogr. Sect. B-Structural Sci.* **1977**, *33*, 1696–1700.
291   9.   Fukuda, K.; Ito, S. Improvement in reactivity and grindability of belite-rich cement by remelting reaction.
292   *J. Am. Ceram. Soc.* **1999**, *82*, 2177–2180.
293   10.   Cuberos, A. J. M.; De la Torre, A. G.; Martin-Sedeno, M. C.; Moreno-real, L.; Merlini, M.; Ordonez, L. M.;
294   Aranda, M. A. G.; De, Á. G.; Martín-sedeño, M. C.; Ordónez, L. M. Phase development in conventional and
295   active belite cement pastes by Rietveld analysis and chemical constraints. *Cem. Concr. Res.* **2009**, *39*, 833–
296   842, doi:10.1016/j.cemconres.2009.06.017.
297   11.   Cuberos, A. J. M.; De la Torre, A. G.; Alvarez-Pinazo, G.; Martin-Sedeno, M. C.; Schollbach, K.; Pollmann,

298 H.; Aranda, M. A. G. Active Iron-Rich Belite Sulfoaluminate Cements: Clinkering and Hydration. *Environ.*
299 *Sci. Technol.* **2010**, *44*, 6855–6862, doi:10.1021/es101785n.

300 12. ElDidamony, H.; Sharara, A. M.; Helmy, I. M.; ElAleem, S. A. Hydration characteristics of beta-C2S in the
301 presence of some accelerators. *Cem. Concr. Res.* **1996**, *26*, 1179–1187.

302 13. Yang, H. G.; Sun, C. H.; Qiao, S. Z.; Zou, J.; Liu, G.; Smith, S. C.; Cheng, H. M.; Lu, G. Q. Anatase TiO2
303 single crystals with a large percentage of reactive facets. *Nature* **2008**, *453*, 638–641, doi:10.1038/nature06964.

304 14. Manzano, H.; Pellenq, R. J. M.; Ulm, F.-J.; Buehler, M. J.; van Duin, A. C. T. Hydration of Calcium Oxide
305 Surface Predicted by Reactive Force Field Molecular Dynamics. *Langmuir* **2012**, *28*, 4187–4197,
306 doi:10.1021/la204338m.

307 15. Raymand, D.; van Duin, A. C. T. T.; Spångberg, D.; Goddard, W. a.; Hermansson, K.; Spangberg, D. Water
308 adsorption on stepped ZnO surfaces from MD simulation. *Surf. Sci.* **2010**, *604*, 741–752,
309 doi:10.1016/j.susc.2009.12.012.

310 16. Stack, A. G.; Raiteri, P.; Gale, J. D. Accurate Rates of the Complex Mechanisms for Growth and Dissolution
311 of Minerals Using a Combination of Rare-Event Theories. *J. Am. Chem. Soc.* **2011**, *134*, 11–14,
312 doi:10.1021/ja204714k.

313 17. De Leeuw, N. H.; Parker, S. C. Molecular-dynamics simulation of MgO surfaces in liquid water using a
314 shell-model potential for water. *Phys. Rev. B* **1998**, *58*, 13901–13908, doi:10.1103/PhysRevB.58.13901.

315 18. de Leeuw, N. H.; Parker, S. C.; Catlow, C. R. a.; Price, G. D.; Leeuw, N. H. De Modelling the effect of water
316 on the surface structure and stability of forsterite. *Phys. Chem. Miner.* **2000**, *27*, 332–341,
317 doi:10.1007/s002690050262.

318 19. Cicero, G.; Grossman, J. C.; Catellani, A.; Galli, G. Water at a Hydrophilic Solid Surface Probed by Ab initio
319 Molecular Dynamics: Inhomogeneous Thin Layers of Dense Fluid. *J. Am. Chem. Soc.* **2005**, *127*, 6830–6835,
320 doi:10.1021/ja042963u.

321 20. Manzano, H.; Durgun, E.; López-Arbeloa, I.; Grossman, J. C. J. C. Insight on Tricalcium Silicate Hydration
322 and Dissolution Mechanism from Molecular Simulations. *ACS Appl. Mater. Interfaces* **2015**, *7*, 14726–14733,
323 doi:10.1021/acsami.5b02505.

324 21. Manzano, H.; Durgun, E.; Abdolhosseine Qomi, M. J.; Ulm, F.-J.; Pellenq, R. J. M.; Grossman, J. C. Impact
325 of Chemical Impurities on the Crystalline Cement Clinker Phases Determined by Atomistic Simulations.
326 *Cryst. Growth Des.* **2011**, *11*, 2964–2972, doi:10.1021/cg200212c.

327 22. Durgun, E.; Manzano, H.; Pellenq, R. J. M.; Grossman, J. C. Understanding and Controlling the Reactivity
328 of the Calcium Silicate phases from First Principles. *Chem. Mater.* **2012**, *24*, 1262–1267,
329 doi:10.1021/cm203127m.

330 23. Durgun, E.; Manzano, H.; Kumar, P. V. V; Grossman, J. C. J. C. The Characterization, Stability, and
331 Reactivity of Synthetic Calcium Silicate Surfaces from First Principles. *J. Phys. Chem. C* **2014**, *118*, 15214–
332 15219, doi:10.1021/jp408325f.

333 24. Huang, J.; Valenzano, L.; Singh, T. V.; Pandey, R.; Sant, G. Influence of (Al, Fe, Mg) Impurities on Triclinic
334 Ca3SiO5: Interpretations from DFT Calculations. *Cryst. Growth Des.* **2014**, *14*, 2158–2171,
335 doi:10.1021/cg401647f.

336 25. Huang, J.; Wang, B.; Yu, Y.; Valenzano, L.; Bauchy, M.; Sant, G. Electronic Origin of Doping-Induced
337 Enhancements of Reactivity: Case Study of Tricalcium Silicate. *J. Phys. Chem. C* **2015**, *119*, 25991–25999,
338 doi:10.1021/acs.jpcc.5b08286.

339 26. Mishra, R. K.; Flatt, R. J.; Heinz, H. Force Field for Tricalcium Silicate and Insight into Nanoscale Properties:
340 Cleavage, Initial Hydration, and Adsorption of Organic Molecules. *J. Phys. Chem. C* **2013**, *117*, 10417–10432,

doi:10.1021/jp312815g.

27. Wang, Q.; Guo, Y.; Manzano, H.; Lopez-Arbeloa, I.; Shen, X.; Li, F. First-principles study of water adsorption and dissociation on β-C2S (100). In *RILEM InternationalSymposium on Concrete Modeling-CONMOD 2014*; RILEM publications, 2014.

28. Wang, Q.; Manzano, H.; Guo, Y.; Lopez-Arbeloa, I.; Shen, X. Hydration Mechanism of Reactive and Passive Dicalcium Silicate Polymorphs from Molecular Simulations. *J. Phys. Chem. C* **2015**, *119*, 19869–19875, doi:10.1021/acs.jpcc.5b05257.

29. Wang, Q.; Li, F.; Shen, X.; Shi, W.; Li, X.; Guo, Y.; Xiong, S.; Zhu, Q. Relation between reactivity and electronic structure for α′L-, β- and γ-dicalcium silicate: A first-principles study. *Cem. Concr. Res.* **2014**, *57*, 28–32, doi:10.1016/j.cemconres.2013.12.004.

30. Mumme, W. G.; Hill, R. J.; Bushnellwye, G.; Segnit, E. R. Rietveld Crystal-Structure Refinements, Crystal-Chemistry and Calculated Powder Diffraction Data for the Polymorphs of Dicalcium Silicate and Related Phases. *Neues Jahrb. Fur Mineral.* **1995**, *169*, 35–68.

31. Delley, B. From molecules to solids with the DMol3 approach. *J. Chem. Phys.* **2000**, *113*, 7756–7764.

32. Perdew, J. P.; Burke, K.; Ernzerhof, M. Generalized gradient approximation made simple. *Phys. Rev. Lett.* **1996**, *77*, 3865–3868.

33. Monkhorst, H. J.; Pack, J. D. Special points for Brillouin-zone integrations. *Phys. Rev. B* **1976**, *13*, 5188–5192.

34. Neugebauer, J.; Scheffler, M. Adsorbate-substrate and adsorbate-adsorbate interactions of Na and K adlayers on Al (111). *Phys. Rev. B* **1992**, *46*, 16067.

35. Momma, K.; Izumi, F. VESTA: a three-dimensional visualization system for electronic and structural analysis. *J. Appl. Crystallogr.* **2008**, *41*, 653–658, doi:10.1107/s0021889808012016.

36. Machesky, M. L.; Predota, M.; Wesolowski, D. J.; Vlcek, L.; Cummings, P. T.; Rosenqvist, J.; Ridley, M. K.; Kubicki, J. D.; Bandura, A. V; Kumar, N. Surface protonation at the rutile (110) interface: explicit incorporation of solvation structure within the refined MUSIC model framework. *Langmuir* **2008**, *24*, 12331–12339.

37. Allen, J. P.; Parker, S. C.; Price, D. W. Atomistic Simulation of the Surface Carbonation of Calcium and Magnesium Oxide Surfaces. *J. Phys. Chem. C* **2009**, *113*, 8320–8328, doi:10.1021/jp810885m.

38. Bolis, V.; Fubini, B.; Marchese, L.; Martra, G.; Costa, D. Hydrophilic and hydrophobic sites on dehydrated crystalline and amorphous silicas. *J. Chem. Soc. Faraday Trans.* **1991**, *87*, 497–505, doi:10.1039/FT9918700497.

39. Grabowski, S. J. Hydrogen bonding strength—measures based on geometric and topological parameters. *J. Phys. Org. Chem.* **2004**, *17*, 18–31, doi:10.1002/poc.685.

40. Duque-Redondo, E.; Manzano, H.; Epelde-Elezcano, N.; Martínez-Martínez, V.; López-Arbeloa, I. Molecular Forces Governing Shear and Tensile Failure in Clay-Dye Hybrid Materials. *Chem. Mater.* **2014**, *26*, 4338–4345, doi:10.1021/cm500661d.

41. Hirshfeld, F. L. Bonded-atom fragments for describing molecular charge densities. *Theor. Chim. Acta* **1977**, *44*, 129–138.

42. Grabowski, S. J. What Is the Covalency of Hydrogen Bonding? *Chem. Rev.* **2011**, *111*, 2597–2625, doi:10.1021/cr800346f.

43. Elgabarty, H.; Khaliullin, R. Z.; Kühne, T. D. Covalency of hydrogen bonds in liquid water can be probed by proton nuclear magnetic resonance experiments. *Nat. Commun.* **2015**, *6*.

44. Juilland, P.; Gallucci, E.; Flatt, R.; Scrivener, K. Dissolution theory applied to the induction period in alite hydration. *Cem. Concr. Res.* **2010**, *40*, 831–844, doi:10.1016/j.cemconres.2010.01.012.